Synthesis of dihydrocarvone over dendritic ZSM-5 Zeolite: A comprehensive study of experimental, kinetics, and computational insights

Gallego-Villada, Luis A.; Perez-Sena, Wander Y.; Sánchez-Velandia, Julián E.; Cueto, Jennifer; del Mar Alonso-Doncel, María; Wärmå, Johan; Mäki-Arvela, Päivi; Alarcón, Edwin A.; Serrano, David P.; Murzin, Dmitry Yu

Published in:
Chemical Engineering Journal

DOI:
10.1016/j.cej.2024.155377

Published: 15/10/2024

Document Version
Final published version

Document License
CC BY

Chemical Engineering Journal 498 (2024) 155377

Contents lists available at ScienceDirect

Chemical Engineering Journal

journal homepage: www.elsevier.com/locate/cej

Synthesis of dihydrocarvone over dendritic ZSM-5 Zeolite: A comprehensive study of experimental, kinetics, and computational insights

Luis A. Gallego-Villada [a,b,*], Wander Y. Perez-Sena [a], Julián E. Sánchez-Velandia [c], Jennifer Cueto [d], María del Mar Alonso-Doncel [d], Johan Wärmå [a], Päivi Mäki-Arvela [a], Edwin A. Alarcón [b], David P. Serrano [d,e,**], Dmitry Yu. Murzin [a,*]

[a] Laboratory of Industrial Chemistry and Reaction Engineering, Johan Gadolin Process Chemistry Centre, Åbo Akademi University, Henriksgatan 2, 20500 Turku/Åbo, Finland
[b] Environmental Catalysis Research Group, Chemical Engineering Faculty, Universidad de Antioquia, Medellín, Colombia
[c] Sustainable and Supramolecular Research Group, Universidad Jaume I, Av. Vicent Sos Baynot, s/n, 12006, Castelló de la Plana, Spain
[d] Thermochemical Processes Unit, IMDEA Energy Institute, Avda. Ramón de la Sagra, 3, 28935, Móstoles, Madrid, Spain
[e] Chemical and Environmental Engineering Group, Rey Juan Carlos University, c/Tulipán s/n, 28933, Móstoles, Madrid, Spain

ARTICLE INFO

Keywords:
ZSM-5
Dendritic zeolite
Limonene epoxide
Dihydrocarvone
Kinetic modeling
Density Functional Theory (DFT)

ABSTRACT

This study explores the isomerization of limonene-1,2-epoxide (LE) from kinetic and mechanistic viewpoints, using a dendritic ZSM-5 zeolite (d-ZSM-5) as a highly selective catalyst for the formation of dihydrocarvone (DHC) in the form of diastereoisomers (*cis* + *trans*). Ethyl acetate, a green solvent, was used at mild reaction temperatures (50—70 °C). DHC, which can also be extracted from caraway oil, is widely used as an intermediate for epoxylactone production and as a constituent in flavors and perfumes. Kinetic modeling of LE isomerization was performed using a reaction network with eight parallel reactions and the corresponding rate equations, derived from the assumption of the rate-limiting surface reactions. The large standard errors in the statistical results of some kinetic parameters of the initial data fitting suggested that three of those reactions can be neglected to describe the kinetic model more accurately. This refinement resulted in standard errors in the kinetic parameters lower than ca. 11 %, confirming the statistical reliability of the modified kinetic model. Activation energies of 41.1 and 162 kJ/mol were estimated for the formation of *cis*-DHC and *trans*-DHC, respectively. Density Functional Theory (DFT) calculations revealed the preferred pathway for both *cis* and *trans*-LE conversion to DHC and carveol. The rate-determining step, carbocation formation (ΔEact = 234 kJ/mol), precedes near-instantaneous dihydrocarvone formation under the studied conditions.

1. Introduction

Terpenes and terpenoids, such as e.g. dihydrocarvone (DHC), are useful as intermediates or final products in various application areas, including fragrances, cosmetics, and pharmaceuticals [1–3]. Monoterpenes, being among the most numerous and structurally diverse natural products, can be extracted by distillation of various biomass sources [4]. Limonene is a monocyclic terpene found in large quantities in numerous essential oils [5] and is the major constituent (91–96 wt%) of pressed orange-peel oil [6]. Oxidation of limonene gives epoxides, glycols, ketones, and alcohols, among other compounds of significant interest in green and sustainable chemistry [4,7–10]. Through the isomerization of monoterpenes epoxides derived from biomass, many substances with potential pharmaceutical applications can be obtained.

1,2-Epoxy limonene (LE) is an attractive organic compound that, under acidic conditions, is isomerized into valuable fine chemicals, such as dihydrocarvone (*cis* + *trans*), carveol, and carvenone (Fig. 1). Dihydrocarvone in turn is used in the synthesis of flavors and perfumes [11], providing numerous precursors like epoxylactones, which serve as intermediates in ring-opening polymerizations [12]. Additionally, this monoterpenoid is naturally found in caraway oil [13] and is used in the synthesis of dispiro-1,2,4,5-tetraoxanes, which exhibit potent anti-

* Corresponding author at: Laboratory of Industrial Chemistry and Reaction Engineering, Johan Gadolin Process Chemistry Centre, Åbo Akademi University, Henriksgatan 2, 20500 Turku/Åbo, Finland.
** Corresponding author at: Thermochemical Processes Unit, IMDEA Energy Institute, Avda. Ramón de la Sagra, 3, 28935, Móstoles, Madrid, Spain
E-mail addresses: alfonso.gallego@udea.edu.co (L.A. Gallego-Villada), david.serrano@imdea.org (D.P. Serrano), dmitry.murzin@abo.fi (D.Yu. Murzin).

https://doi.org/10.1016/j.cej.2024.155377
Received 13 June 2024; Received in revised form 15 August 2024; Accepted 29 August 2024
Available online 7 September 2024

malarial activity [14], and α-cyperone, a eudesmane type sesquiterpenoid compound with potent insecticidal activity [15]. Furthermore, carveol exhibits chemopreventive properties against mammary carcinogenesis [16,17]. Carvenone is also widely used as a constituent in the synthesis of numerous flavors and fragrances [18].

In comparison to pinenes epoxides, isomerization of limonene epoxide has been scarcely studied. The conventional homogeneous catalyst reported for the isomerization of limonene epoxide is $ZnBr_2$, which results in cyclopentanecarboxyaldehyde (CPCA) and DHC as the main products [19]. Generally, LE can be converted in the presence of acidic heterogeneous catalysts [1], including amorphous silica-alumina [20], montmorillonite [18], Keggin-type heteropolyacids [1,21], Fe/SBA-15 [22], Au/TiO_2 [23], and SiO_2-Al_2O_3 [24]. According to these reports, the high reactivity and selectivity of the isomerization route depend strongly on the specific reaction conditions as well as on the catalyst and solvent type. The most critical factors influencing selectivity toward a specific target from limonene epoxide are the type of acid sites (Brønsted, Lewis, or their ratio) and the solvent (polar or non-polar).

Previous catalytic systems have used either toxic solvents such as toluene [20], 1,4-dioxane [21], dichloromethane [21], 1,2-dichloroethane [21], and acetonitrile [22], or very high temperatures (140 °C) [18]. Additionally, those systems exhibited limited yields to DHC as the major product, with the best result (80 % yield) obtained with the Keggin-type heteropolyacid using 1,4-dioxane as the solvent [21]. In our recent study [25], dendritic ZSM-5 zeolites were found to be highly active catalysts for the valorization of monoterpene epoxides, such as internal limonene epoxide, α-pinene epoxide, and β-pinene epoxide, converting them into dihydrocarvone, campholenic aldehyde, and myrtanal, respectively. Notably, a remarkable yield of DHC (63 %, 70 °C, 2 h) was achieved using a benign solvent like ethyl acetate and a relatively low temperature, with dendritic ZSM-5 zeolite (d-ZSM-5). Table 1 presents a comparison based on turnover frequency (TOF) value for different heterogeneous catalysts, calculated based on the total acidity of the materials. Dendritic ZSM-5 zeolite exhibited superior activity in the isomerization route with a TOF of 4.4 min^{-1}, significantly higher than that of other catalysts.

These findings validate the high interest and potential of dendritic zeolites due to their vast range of possible applications as catalysts [26]. These zeolites exhibit three-dimensional branched superstructures marked by exceptional accessibility, owing to a highly interconnected network of radially oriented mesopores [26,27], which facilitates the rearrangement of monoterpene epoxides into high-value-added products.

The opening of limonene epoxide is a crucial reaction for research from both catalytic and molecular perspectives due to its wide applications in fine chemistry. Despite the significance of this reaction, there is a lack of detailed information about key parameters necessary for understanding the reaction mechanism, including bonding interactions, transition states, formation of intermediates, and kinetics. Both experimental and theoretical reports in the open literature fail to provide a comprehensive description of the reaction mechanism or offer molecular-based explanations for the observed selectivity in limonene epoxide isomerization. This knowledge gap hinders the scaling up of the process and an in-depth understanding of its chemical nature.

Table 1
Comparison of TOF using several catalysts in the limonene-1,2-epoxide isomerization.

Catalyst	Solvent	Reaction conditions	TOF[b] (min^{-1})	Reference
ZSM-5	Ethyl acetate	13 mmol L^{-1}, 75 mL of total volume, 115 mg of catalyst, 70 °C, 520–530 rpm, N_2 atmosphere	0.6	[25]
h-ZSM-5	Ethyl acetate		1.6	
d-ZSM-5/4d	Ethyl acetate		4.4	
d-ZSM-5/7d	Ethyl acetate		2.3	
3.9Fe/SBA15[a]	Toluene	0.25 mmol of substrate, 1 mL of solvent, 70 °C, 750 rpm, 10 mg of catalyst	0.46	[22]
	Ethyl acetate		0.29	
	Acetonitrile		0.12	
	Acetone		0.35	
	THF		0.12	
	1,4-Dioxane		0.17	
	Tert-butanol		0.12	
	Cyclohexane		0.23	
	Hexane		0.23	

[a] The values represent the metal loading (% wt.).
[b] TOF was calculated as $(n_{i,LE} - n_{f,LE})/(\Delta t \cdot TA \cdot W)$ where $n_{i,LE}$ and $n_{f,LE}$ correspond to moles of LE at time 0 min and 5 min, respectively, Δt is the time interval, W is the catalyst weight, and TA is the total acidity referred to the sum of Brønsted and Lewis acidity of the catalyst.

Hence, the present study is aimed to perform the kinetic modeling and mechanistic exploration of the limonene-1,2-epoxide isomerization over dendritic ZSM-5 zeolite, selecting the catalyst sample that showed the best performance in our recent report on dendritic zeolites [25]. This material exhibited a high selectivity for *cis/trans*-dihydrocarvone, using mild reaction conditions and a green solvent, ethyl acetate. The current work focuses on successfully describing the reaction pathway through the proposed reaction network, explained by the very good accuracy of the kinetic model to fit the experimental data collected under varying substrates (*cis*-LE, *trans*-LE, and mixture-LE) and temperatures. Density functional theory (DFT) calculations were also conducted to elucidate the mechanism of epoxide rearrangement.

2. Experimental section

2.1. Materials

Commercial reagents were used in the experiments without further processing. Reagents for the synthesis of dendritic material were aluminum isopropoxide (AlP, 98 wt%, Sigma-Aldrich); tetrapropylammonium hydroxide (TPAOH, 40 wt% in water, Sigma-Aldrich);

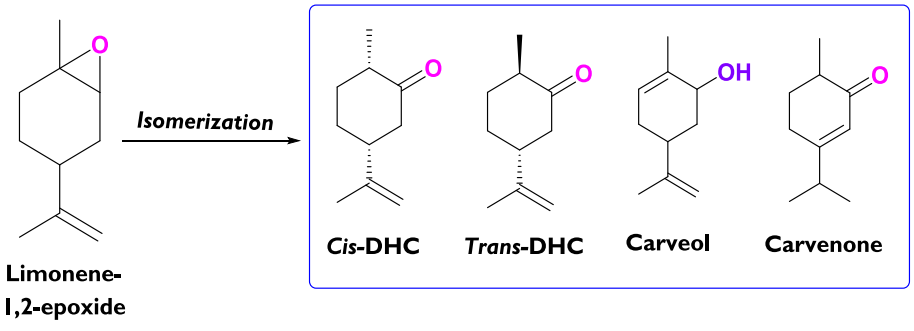

Fig. 1. Rearrangement of limonene-1,2-epoxide into high added-value products.

tetraethyl orthosilicate (TEOS, 98 wt%, Sigma-Aldrich); dimethyloctadecyl [3-(trimethoxysilyl) propil] ammonium chloride (TPOAC, 42 wt% in methanol, Sigma-Aldrich); N-[3-(Trimethoxysilyl)propyl]aniline (Ph-A, 98 %, Sigma-Aldrich). Reagents for the catalytic tests were (+)-limonene-1,2-epoxide (mixture of isomers *cis* + *trans*, ≥ 97 wt%, Sigma-Aldrich), *cis*-(−)-limonene-1,2-epoxide (98 wt%, Sigma-Aldrich), *trans*-limonene-1,2-epoxide (97.5 wt%, Sigma-Aldrich), ethyl acetate (anhydrous, 99.8 wt%, Sigma-Aldrich), and nitrogen (99.999 %, Woikoski). Some standards utilized for the quantification through the multipoint calibration curves were D-dihydrocarvone (≥ 97 wt%, mixture of isomers, Sigma-Aldrich), L-carveol (mixture of *cis* and *trans*, ≥ 95 wt%, Sigma-Aldrich), (1*S*,2*S*,4*R*)-(+)-limonene-1,2-diol (≥ 97 wt%, Sigma-Aldrich), and *p*-cymene (≥ 90 wt%, Fluka).

2.2. Synthesis of dendritic ZSM-5 zeolite

The detailed methodology for the synthesis of dendritic ZSM-5 materials has been previously reported in our recent work [25]. The dendritic ZSM-5 sample was synthesized by initially mixing finely milled AlP with TPAOH and distilled water at 300 rpm and room temperature in a round bottom flask until AIP was completely dissolved. Subsequently, an appropriate amount of TEOS, was added dropwise while the flask was submerged in an ice bath. This mixture was then stirred at room temperature for 42 h to ensure complete hydrolysis of TEOS. The initial precursor solution had a molar composition of 1 Al_2O_3: 60 SiO_2: 11 TPAOH: 1500 H_2O. The hydrolysis by-products, primarily alcohols, were removed using a rotatory evaporator at 100 mbar and 50 °C. The clear precursor solution underwent pre-crystallization under reflux with stirring at 300 rpm and 90 °C for 20 h. Following this, the flask was cooled in an ice bath and a 5 mol% of TPOAC relative to the initial silicon content was added dropwise to the synthesis gel, which was then stirred in the ice bath for 6 h. Hydrothermal crystallization of the synthesis gel was conducted by transferring it to a Teflon-lined reactor, which was sealed and maintained at 150 °C for 4 days. Post-crystallization, the autoclaves were rapidly cooled in an ice bath to abruptly halt the process. This procedure yielded two phases from the dendritic synthesis gel after 4 days: a whitish supernatant gel and a white solid at the bottom of the Teflon container. The white solid, containing the dendritic zeolite sample, was mechanically separated, washed with distilled water, centrifuged at 11000 rpm three times, and dried at 100 °C overnight. The resulting solid was designated as d-ZSM-5. This material was calcined in a two-step process using Ar and synthetic air as carrier gases for the first and second steps, respectively, following a reported procedure [28].

2.3. Catalysts characterization

In our recent work [25], we extensively characterized the dendritic ZSM-5 zeolite using an arsenal of modern physico-chemical methods, including X-ray diffraction (XRD), argon physisorption, transmission electron microscopy (TEM), high resolution-TEM, inductively coupled plasma – optical emission spectrometry (ICP-OES), pyridine-FTIR, solid-state ^{27}Al MAS NMR, DTBPy/FTIR, and TGA analyses.

2.4. Catalytic tests

The isomerization of limonene-1–2-epoxide over a heterogeneous catalyst was conducted in a batch glass reactor (total liquid volume of 75 mL) under a nitrogen atmosphere. The reactor was equipped with a N_2 feeding system, a thermocouple, a sampling valve, and a condenser. Small catalyst particles (<75 μm) were used to minimize internal mass transfer limitations. The catalytic tests were performed using a high liquid volume-to-catalyst mass ratio and vigorous agitation (530 rpm) to suppress external mass-transfer limitations [29,30].

In a typical run, 115 mg of catalyst was heated at 250 °C for 30 min under a nitrogen atmosphere to avoid the physisorption of water. Subsequently, 1 mmol of epoxide was added to the pre-heated ethyl acetate at 70 °C to reach a total liquid volume of 75 mL. The samples of 0.4 mL were collected at regular intervals using a syringe with 0.45 μm filters to analyze the reaction kinetics using an Agilent Technologies GC-6890 N gas chromatograph equipped with a DB-1 column (30 m length x 250 μm internal diameter x 0.50 μm film thickness), an FID detector, and an autosampler.

Helium was used as the carrier gas at a pressure of 0.12 MPa and a flow rate of 1.5 mL min^{-1} with a split ratio of 10:1. The detector temperature was set to 280 °C, and the injection volume was 1 μL. The oven-temperature program started at 60 °C, ramping to 100 °C at a rate of 20 °C min^{-1}, followed by an increase to 200 °C at 10 °C min^{-1}, and holding for 1 min. The nature of the products was further confirmed using an Agilent GC/MS 6890 N/5973 N equipped with a DB-1 capillary column (30 m length x 250 μm internal diameter x 0.5 μm film thickness).

The limonene-1,2-epoxide conversion (X_{LE}), and selectivity to the product i (S_i) were calculated based on the Eqs. (1) and (2).

$$X_{LE}(\%) = \frac{n_{LE,0} - n_{LE,t}}{n_{LE,0}} * 100 \quad (1)$$

$$S_i(\%) = \frac{n_{i,t}}{n_{LE,0} - n_{LE,t}} * 100 \quad (2)$$

Where $n_{LE,0}$, $n_{LE,t}$, and $n_{i,t}$ refer to the initial moles of LE, the moles of LE after time *t*, and the moles of the product i after time *t* in the reaction mixture, respectively. The concentrations of the species were determined from multipoint calibration curves. The initial reaction rate for limonene-1,2-epoxide was calculated using Eq. (3), where $n_{LE,f}$ correspond to moles of LE after 5 min, Δt is the time interval, and W is the catalyst weight.

$$r_{0,LE} = \frac{n_{LE,0} - n_{LE,f}}{\Delta t * W} \quad (3)$$

2.5. Computational methodology

To optimize minimum structures and transition states, the DFT method was employed, specifically utilizing the hybrid functional B3LYP, known for its balance between accuracy and computational efficiency [31]. Additionally, Grimme's empirical dispersion correction (D3) was incorporated to prevent the underestimation of energy [32,33]. The combination of the B3LYP hybrid functional and Grimme's dispersion correction (D3) has become a widely used approach in computational chemistry, owing to its ability to accurately describe various molecular properties [34]. While B3LYP is a well-established functional for predicting molecular geometries and energies, weak dispersion forces, crucial for numerous non-covalent interactions, tend to be underestimated [35]. This limitation is addressed by Grimme's D3 correction, which explicitly incorporates dispersion interactions into the calculation, significantly enhancing the accuracy of overall energy and structural predictions [32,33]. This combination of B3LYP and D3 has been demonstrated to be effective for diverse systems, including small molecules, polymers, and biological macromolecules. The 6–31++G(d, p) basis set was also used for these calculations. The effect of temperature (343 K) was considered during computational calculations.

To validate the calculated structures, frequency analysis was performed, checking for non-imaginary frequencies for stable geometries and a single imaginary frequency for transition states. This analysis was corroborated by calculating analytic second derivatives. The Intrinsic Reaction Coordinate (IRC) was employed to connect the transition state structures to the intermediates, products, and reactants. To consider solvent effects (ethyl acetate), the Conductor-like Polarizable Continuum Model (CPCM) was applied during optimization calculations. This model utilizes a set of overlapping spheres to represent the solute cavity and employs a continuous surface charge formalism to ensure reaction

continuity and robustness [36]. In this study, H_3O^+ was used as the acid species instead of directly mimicking the structure of a dendritic zeolite. This decision was made because H_3O^+ serves as a representative model for the typical Brønsted acid site in the catalyst [37]. The initial reference was established as the sum of limonene epoxide (*cis* or *trans*) and the Brønsted acid H_3O^+. Topological analysis of the electronic density was conducted using the AIMALL software.

2.6. Kinetic modeling

2.6.1. Reaction network

The reaction network for the isomerization of limonene-1,2-epoxide over d-ZSM-5 is proposed according to our results (Table 2 and Table S1) [25], as illustrated in Fig. 2. Primarily, *cis*-limonene-1,2-epoxide (A) is transformed into *cis*-dihydrocarvone (C), and *trans*-limonene-1,2-epoxide (B) gives *trans*-dihydrocarvone (D). Additionally, A and B undergo parallel reactions, resulting in carveol (E) and 1,3,4-trimethyl-3-cyclohexen-1-carboxaldehyde (F). The formation of the alcohol (E) can be explained by a concerted mechanism of *cis*-LE and *trans*-LE over Au/TiO_2 as a catalyst [23]. Products 4, 5, 6, and 7 are collectively labeled as 'Others' due to their low concentrations relative to the previously mentioned products. This kinetic study aims to investigate the determining steps and possible reaction pathways of the isomerization of limonene-1,2-epoxide over the dendritic ZSM-5 zeolite. It is noteworthy that all routes primarily involve the isomerization of epoxides ($C_{10}H_{16}O$), except for their slow dehydration into product 6 ($C_{10}H_{14}$).

2.6.2. Kinetic equations for a batch reactor

The reaction rate expressions are presented in Eqns. (4) and (5), with detailed derivations available in the supporting information (section 1). The surface reactions are assumed to be irreversible, with k and K representing the reaction rate and adsorption equilibrium constants, respectively. Reaction constants are calculated using the modified Arrhenius equation, Eq. (6), where k_{ref} refers to the reaction rate constant at an average temperature ($T_{av} = 60$ °C), E_a denotes the activation energy, and R represents the gas constant. On the other hand, the adsorption constants can be considered constant within the temperature range studied in this contribution (50–70 °C) [7,38,39].

$$r_i = \frac{k_i C_A}{1 + K_A C_A + K_B C_B + K_C C_C + K_D C_D + K_E C_E + K_F C_F} \quad (i = 1, 3, 5, 7) \tag{4}$$

$$r_j = \frac{k_j C_B}{1 + K_A C_A + K_B C_B + K_C C_C + K_D C_D + K_E C_E + K_F C_F} \quad (j = 2, 4, 6, 8) \tag{5}$$

$$k = k_{ref} e^{-\frac{E_a}{R}\left(\frac{1}{T} - \frac{1}{T_{av}}\right)} \tag{6}$$

The mole balance for the species in the liquid phase in the batch reactor is represented by Eq. (7), where C_i is the concentration of species i, m_{cat} is the catalyst mass, V_R is the reaction volume, and R_i is the generation rate for species i, as shown in Table 3.

Table 2
Experimental conditions for the kinetic modeling over d-ZSM-5[a].

Entry	Substrate	W (mg)	T (°C)
1	*Cis*-LE	115.8	70
2	*Trans*-LE	116.3	70
3	Mixture-LE	116.3	50
4	Mixture-LE	115.1	60
5	Mixture-LE	115.5	70

[a] 13 mmol/L, 75 mL of total volume, anhydrous ethyl acetate as a solvent, 520 rpm, N_2 atmosphere.

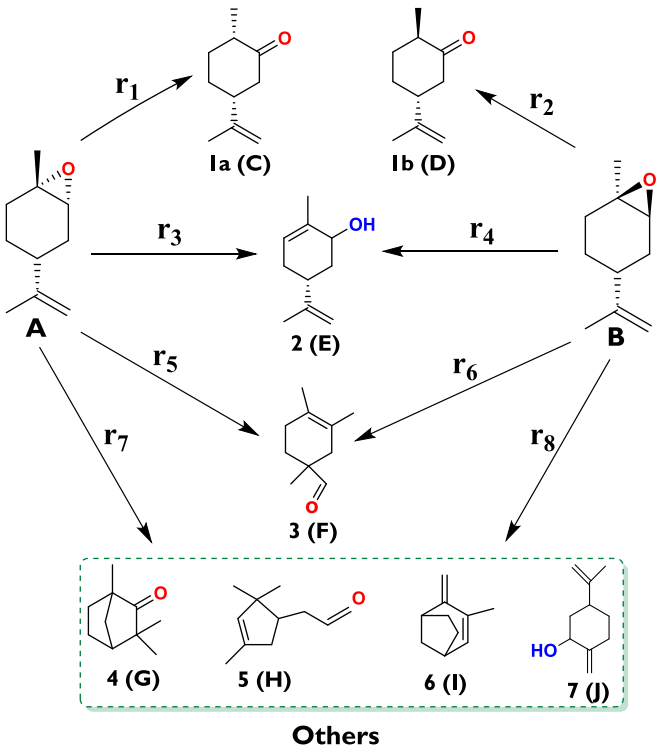

Fig. 2. Reaction network for the isomerization of limonene-1,2-epoxide (**A:** *cis* configuration and **B:** *trans*-configuration) over d-ZSM-5.

Table 3
Production rate for each species i.

Specie	Production rate (R_i)
Cis-limonene-1,2-epoxide (A)	$-r_1 - r_3 - r_5 - r_7$
Trans-limonene-1,2-epoxide (B)	$-r_2 - r_4 - r_6 - r_8$
Cis-dihydrocarvone (C)	r_1
Trans-dihydrocarvone (D)	r_2
Carveol (E)	$r_3 + r_4$
Product **3** (F)	$r_5 + r_6$
Others	$r_7 + r_8$

Product **3**: 1,3,4-trimethyl-3-cyclohexen-1-carboxaldehyde.

$$\frac{dC_i}{dt} = \frac{m_{cat}}{V_R} R_i \quad (i = A, B, C, D, E, F, \text{Others}) \tag{7}$$

2.6.3. Parameters estimation

The estimation of parameters through nonlinear regression was conducted using the ModEst modeling and parameter estimation software (section 3 of supporting information) [40,41]. This process involved minimizing the objective function (O.F) by employing the Levenberg-Marquardt algorithm. O.F was formulated as the squared difference between the experimental and calculated values of the concentration of species [7,41], as illustrated in Eq. (8). The determination coefficient (R^2) is a widely used metric for evaluating the goodness of fit, comparing the residual concentration values, as defined by Eq. (9). Here, $C_{j,i,\,Exp}$ and $C_{j,i,\,Calc}$ refer to the experimental and modeled concentrations of the species j for each run i, respectively, while $\overline{C}_{j,i,\,Exp}$ refers to the mean of the experimental concentration data.

$$O.F = \sum_{j}^{N_{com}} \sum_{i=1}^{N_{obs}} \left(C_{j,i,\,Exp} - C_{j,i,\,Calc}\right)^2 \tag{8}$$

$$R^2(\%) = 100\left(1 - \frac{\sum_j^{N_{com}}\sum_{i=1}^{N_{obs}}\left(C_{j,i,\,Exp} - C_{j,i,\,Calc}\right)^2}{\sum_j^{N_{com}}\sum_{i=1}^{N_{obs}}\left(C_{j,i,\,Exp} - \overline{C}_{j,i,\,Exp}\right)^2}\right) \quad (9)$$

3. Results and discussion

3.1. Catalyst properties

The dendritic ZSM-5 sample (d-ZSM-5) herein investigated corresponds with the material showing the best performance as reported in a separated article [25], in which its robustness and full recovery of the catalytic activity through regeneration by air calcination were demonstrated. The main physicochemical properties of this d-ZSM-5 sample are summarized in Fig. 3. XRD pattern (Fig. 3a) shows the typical diffraction peaks of the MFI zeolitic structure, confirming the high crystallinity of the sample. Ar adsorption–desorption isotherm (Fig. 3b), and the derived NL-DFT pore size distribution, denote the presence of a well-defined mesoporosity with a peak maximum at about 5 nm, in addition to the peak corresponding to the MFI zeolitic structure micropores (0.55 nm) and a broad signal extending over the *meso*-macropore border. This singular and complex hierarchical porosity is a consequence of the presence of a dendritic nanostructure in this material.

As shown in the TEM image of Fig. 3c, and as earlier reported [26,27], the dendritic ZSM-5 is formed by particles with sizes between 0.2 – 0.8 μm that consist in branched and radially-oriented aggregates of very small zeolitic nanounits (5 – 10 nm size). Moreover, some vesicles inside the particles can be also appreciated. Therefore, the combination of micropores inside the nanounits, voids existing between the nanounits, and vesicles generate a highly interconnected network of multilevel porosities. This nanoarchitecture provides d-ZSM-5 with outstanding accessibility, as denoted also by its large mesopore-external surface area (360 $m^2\ g^{-1}$) and mesoporosity (about 80 % of the total pore volume). These features have also an effect on the zeolite acidity that is formed by both Brønsted and Lewis acid sites in significant concentration (BAS/LAS=1.4) with a high degree of accessibility [25].

3.2. Catalytic activity

In our recent study [25] the effects of the substrate (*cis*-LE, *trans*-LE, and mixture-LE), solvent polarity, and catalyst robustness were investigated. Herein the focus is on the effect of temperature which is crucial for determining the kinetic parameters, such as pre-exponential factors and activation energy, for all proposed reactions.

A wide range of values has been reported for the temperature of LE conversion over heterogeneous catalysts, such as room temperature [21], 40 °C [1], and 70 °C [22]. In this study, the temperature was investigated in the range of 50–70 °C using anhydrous ethyl acetate as a solvent. Fig. 4a clearly shows that LE conversion increases with the reaction temperature, reaching values of 60 %, 80 %, and 100 % after 2 h at 50 °C, 60 °C and 70 °C, respectively. Additionally, Fig. 4b demonstrates that *cis*-LE is more reactive at higher temperatures, with complete consumption observed after 15 and 60 min of the reaction at 70 and 60 °C, respectively. In the case of 50 °C, even after 2 h, *cis*-LE had not been completely converted.

These results indicate that the reaction proceeds at a low range of temperatures because of the high activity of the dendritic ZSM-5 catalyst. Moreover, both the substrate conversion and cis/trans ratio (Fig. 4a and b) vary sharply when the temperature increases from 60 to 70 °C, evidencing occurrence of a strongly activated process.

The initial reaction rate of the epoxide ($-r_{LE,0}$), calculated under the same reaction conditions (initial molar concentration, agitation speed, and amount of catalyst), can be related to the absolute temperature, as shown in Fig. 4g, to estimate the activation energy (81.4 kJ mol^{-1}) of the epoxide isomerization. This value is very similar to a previously reported activation energy (82 kJ mol^{-1}) for the transformation of limonene epoxide to carvenone, using a Keggin-heteropolyacid catalyst [1].

Selectivity to (*cis* + *trans*)-DHC (Fig. 4c) and carveol (Fig. 4d) is not significantly affected by the temperature given the values ranging

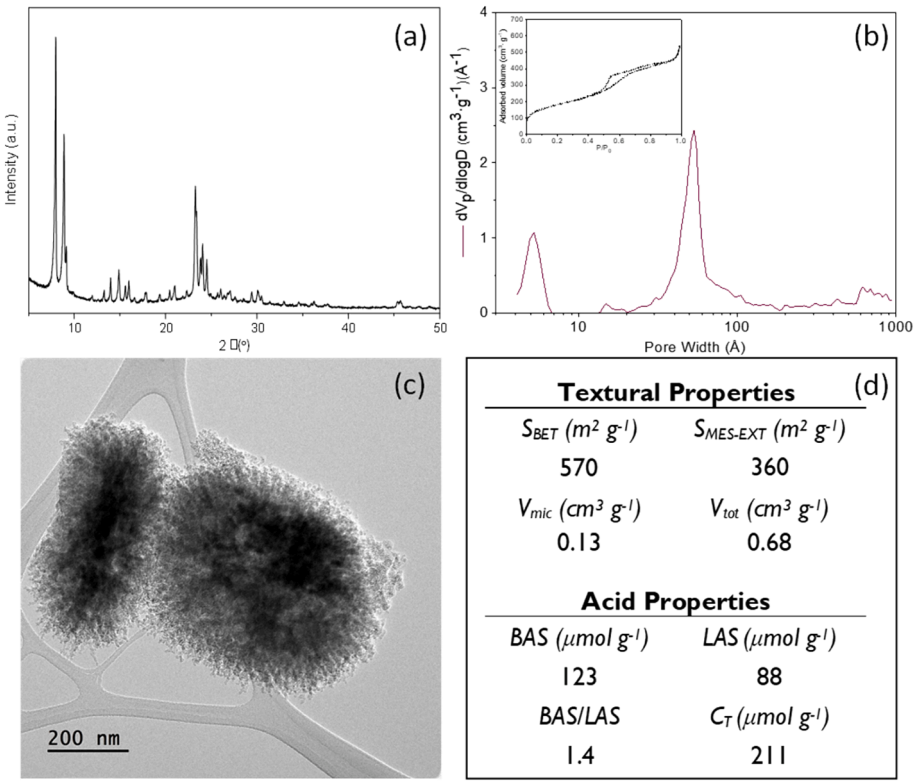

Fig. 3. Summary of the characterization and physico-chemical properties of the calcined d-ZSM-5 sample: **(a)** XRD pattern, **(b)** Ar adsorption–desorption isotherm and NL-DFT pore size distribution (Ar, 87 K), **(c)** TEM image, **(d)** Textural properties and acid features (FTIR-pyridine, evacuation temperature: 250 °C).

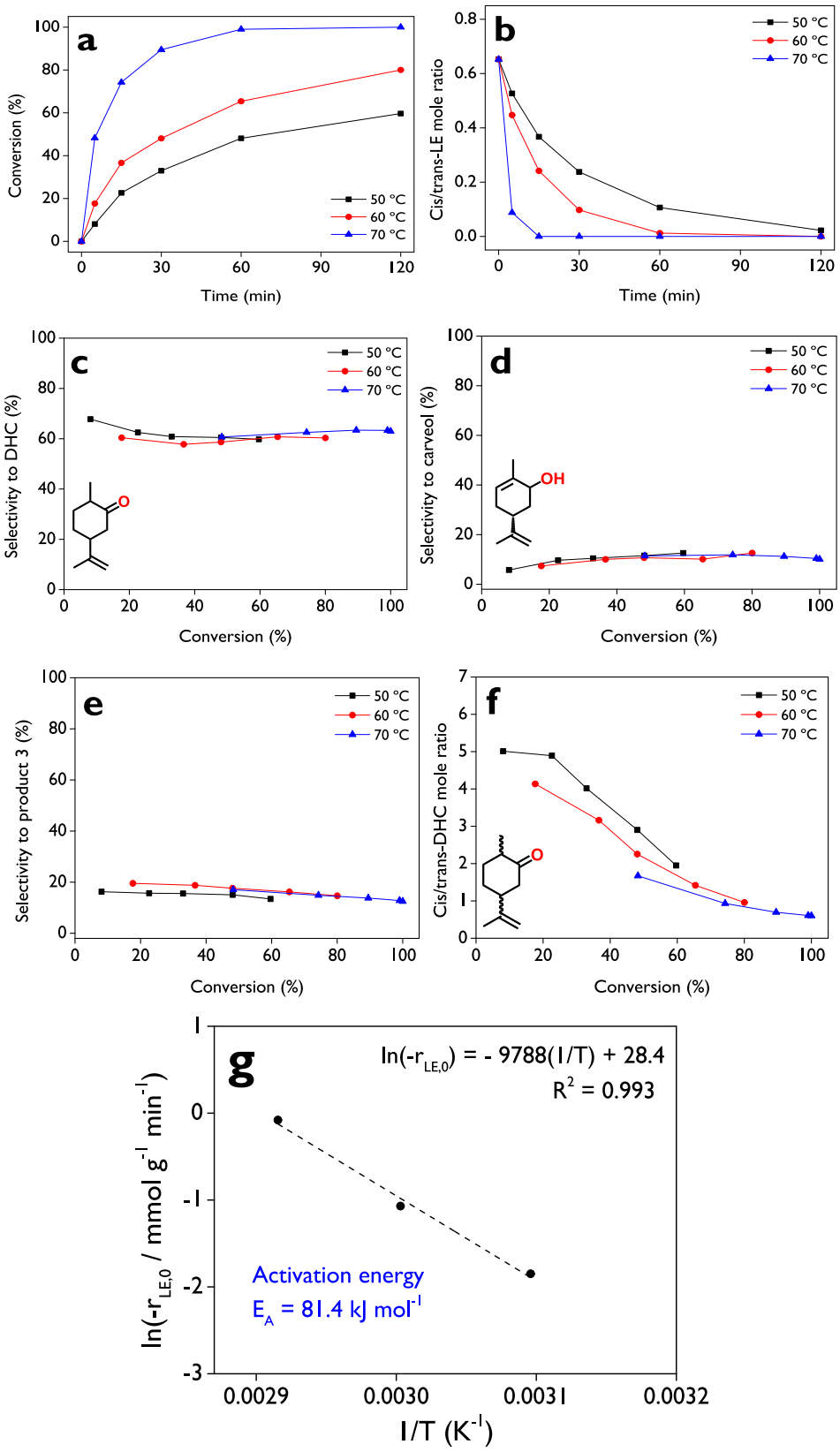

Fig. 4. Effect of the temperature on the LE isomerization over d-ZSM-5. **(a)** LE conversion and **(b)** *cis/trans*-LE molar ratio as a function of the reaction time; **(c)** selectivity to dihydrocarvone, **(d)** selectivity to carveol, **(e)** selectivity to product **3**, and **(f)** *cis/trans* dihydrocarvone molar ratio, as a function of the conversion; **(g)** estimation of the activation energy. **Reaction conditions:** $C_{LE,0}$ = 13 mmol/L, 75 mL of total volume, anhydrous ethyl acetate as a solvent, 115 mg of d-ZSM-5, 520–530 rpm, N_2 atmosphere.

between 60–67 % and 7–12 %, respectively. Selectivity of about 14–20 % to product **3** (Fig. 4e) was reached at 60 and 70 °C, whereas a maximum value of 16 % was achieved at a low temperature (50 °C). The *cis/trans*-DHC molar ratio, shown in Fig. 4f, is reduced as the temperature increases. At 60 % of conversion, values of ca. 1.9, 1.7, and 1.3 were reached at 50, 60, and 70 °C, respectively.

The results with the dendritic zeolite demonstrate its superior activity for the isomerization of limonene-1,2-epoxide compared to other heterogeneous catalysts, such as 3.9 wt% Fe/SBA-15 [22], which exhibited only 15 % conversion using ethyl acetate as a solvent at 70 °C after 1 h. This is significantly lower than the 99 % conversion achieved with dendritic zeolite under the same temperature and at the same reaction time (Fig. 4a). The best conversion reported by the authors for Fe/SBA-15 was 21 % using toluene as the solvent. In terms of selectivity, the values between 42–44 % were achieved with these two solvents, while with d-ZSM-5, selectivity exceeding 60 % were obtained (Fig. 4c). On the other hand, when using a heteropolyacid as a catalyst with toluene as the solvent at 70 °C [1], complete conversion was reached, but with 46 % selectivity to DHC and 34 % selectivity to carvenone after 5 h of reaction. Using dimethyl carbonate as the solvent, the authors reported complete conversion, but with 20 % selectivity to DHC and 68 % selectivity to carvenone.

3.3. Computational calculations

DFT calculations revealed the typical reaction pathway for synthesizing *cis/trans*-dihydrocarvone and *trans*-carveol from *cis/trans*-limonene epoxide (Fig. 5). At the assessed level of theory, no significant differences (~1 kJ mol^{-1}) were observed when the reaction started from either *cis* or *trans*-limonene epoxide. The presented calculations are interconnected, with the initial point of the DFT profile being *trans*-limonene epoxide.

As expected, the initial step in the reaction mechanism involves the approximation of oxygen to the acidic proton in H_3O^+. During this process, the energy decreases to −72 kJ mol^{-1}, indicating significant favorability. It is noteworthy that the C-O bond adjacent to the methylene group increases from 1.45 Å in the initial epoxide to 1.66 Å in **Int1**. This loss of covalence in **int1** is attributed to the formation of an oxonium ion, where the bond distances are slightly larger than the typical C-O bond. Subsequently, a transition state (**TS1**) is observed in which the C-O bond is partially broken, shifting from sp^3 to sp^2 hybridization. The adjacent carbon is minimally affected by **TS1;** however, the angles undergo slight changes, approaching 110°. The energy difference between **Int1** and **TS1** (ΔE_{act} TS1) increases to 234 kJ mol^{-1}. Utilizing the well-defined energies of TS1, the kinetic constant can be estimated.

The calculation of a thermal kinetic constant can be carried out using the Classical Transition State Theory, under the assumption that no trajectories recross the transition state [42]. While this assumption is suitable for systems employing classical mechanics, its application to chemical reactions is entirely invalid. An example illustrating this is the transfer reaction of light atoms, such as hydrogen, which can proceed via tunneling, as observed in both **TS1** and **TS2**. In such cases, the Wigner correction should be considered. A combination of both expressions yields Eq. (10).

$$k = \frac{K_b T}{h} e^{-\frac{\Delta G}{RT}*} \left(1 + \frac{1}{24}\left|\frac{h\nu}{K_b T}\right|^2\right) \quad (10)$$

Where k is the kinetic constant (in s^{-1}) of the transition state, K_b is the Boltzmann's constant (1.38x10^{-23} J K^{-1}), h is the Planck's constant (6.626x10^{-34} J·s), R is the ideal gas constant (8.314 J mol^{-1} K^{-1}), T is the temperature, ΔG is the Gibbs free energy (in kJ/mol), and ν is the frequency of the transition state (in s^{-1}).

By using Eq. (10), the kinetic constant of **TS1** ($\nu = -472$ cm^{-1}) yields a small value of 1.90x10^{-12} s^{-1}. Undoubtedly, the formation of the carbocation (**Int2**) by passing through **TS1** is the determining step in comparison with the upcoming steps. After **TS1**, a significant difference of 246 kJ mol^{-1} is observed concerning the tertiary carbocation (**Int2**). This intermediate is stabilized by hyperconjugation due to the methylene group. In comparison with the preceding **TS1** and **Int1**, the reactivity of the latter is higher because of the band-gap energy obtained as the difference between the HOMO-LUMO frontier orbitals (Table 4). In terms of stability and reactivity, the less stable specie (the most reactive) should be the one with the lowest HOMO-LUMO gap (Pearson's theory [43,44]). By using this well-known correlation for isomerization of

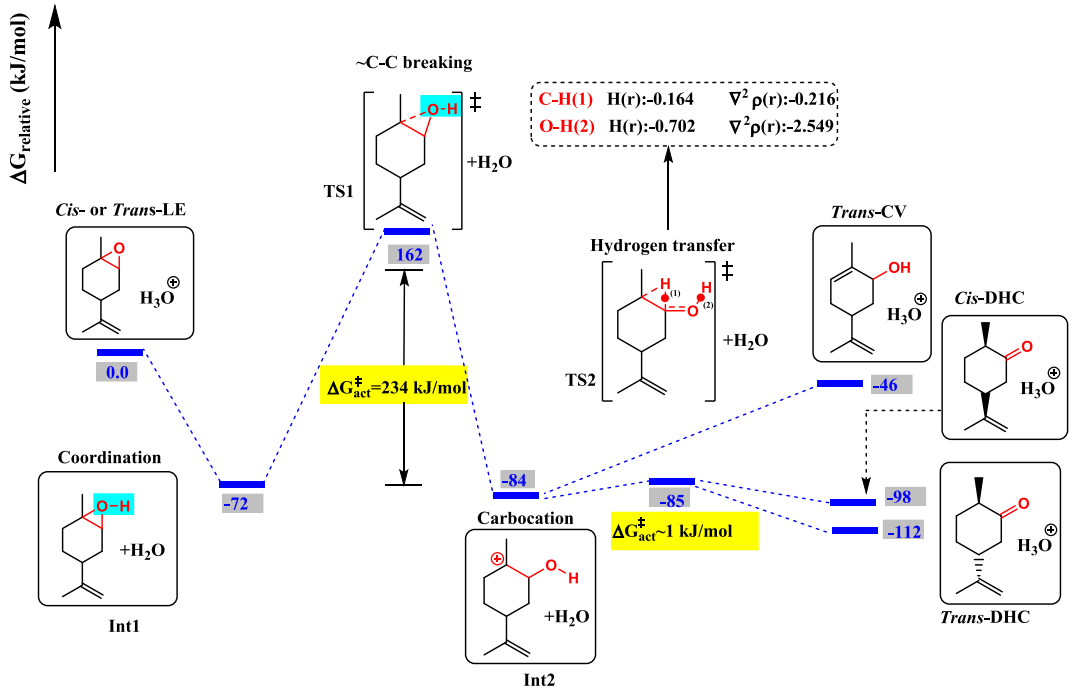

Fig. 5. Calculated diagram for the isomerization of limonene epoxide into *trans*-carveol and *cis/trans*-dihydrocarvone.

Table 4
Band-gap HOMO-LUMO values of the calculated structures.

Structure	Band gap (eV)
Trans-limonene epoxide	6.7
Int1	5.7
Int2	3.2
Trans-carveol	6.3
Trans-DHC	6.0
Cis-DHC	6.0

limonene epoxide, the reactivity of the most relevant structures decreases in the following order: **Int2** > **Int1** > ***Trans/cis*-limonene epoxide**.

After the formation of the intermediate carbocation (**Int2**), the elimination of the adjacent hydrogen results in *trans*-carveol with an overall Gibbs energy of −46 kJ mol^{-1}. In the case of both *cis* and *trans*-DHC, a second transition state (**TS2**) is observed. Specifically, in **TS2,** the hydrogen transfer occurs to the electron-deficient carbon adjacent to the alcohol group. The attached hydrogen to oxygen contributes its electronic pair to form the polarizable C=O bond. The energy difference between **TS2** (ν = -505 cm^{-1}) and **Int2** is only 1 kJ mol^{-1}, yielding a kinetic constant of 1.03 s^{-1}, much faster than for **TS1,** indicating that the formation of **Int2** is evidently the determining step. The formation of both stereochemical configurations of DHC shows that they are thermodynamically favorable, even more so than the synthesis of *trans*-CV, aligning with our experimental results [25]. It is important to highlight that during the thermodynamic calculations, entropic effects were not considered due to their insignificance (<0.042 kJ mol^{-1} K^{-1}).

The low level of *trans*-carveol formation [25] can be attributed to kinetic effects with a minor contribution of thermodynamics. It is evident that *trans*-carveol, on its own, is thermodynamically favorable from *trans/cis*-limonene epoxide. However, starting from the intermediate carbocation (**Int2**), achieving this alcohol becomes challenging due to the thermodynamics constraint of this step (ΔG=38 kJ mol^{-1}). Additionally, elimination of the proton to form the C=C bond is not favored, likely due to the solvent used. Elimination reactions are generally favored in polar protic solvents compared to polar aprotic or non-polar solvents. Moreover, this bond is highly favored with hydrogen abstraction from the least hindered carbon [23]. This preference is the reason why *trans/cis*-DHC is favored over *trans*-CV, not only because of the thermodynamic contribution but also due to kinetic and solvent effects. These factors, together with the typical architecture/geometry of the dendritic zeolite (the latter not considered during the computational calculations), contribute to the observed experimental results [25]. Despite our proposed stepwise mechanism, the literature suggests that *trans*-CV synthesis over Au/TiO_2 can occur via a concerted pathway [23]. In this alternative mechanism, the axially oriented C–H bond on the geminal carbon of the epoxide preferentially reacts over the adjacent methylene group, leading primarily to formation of this alcohol.

The exclusive formation of *trans*-DHC from *trans*-limonene epoxide and *cis*-DHC from *cis*-limonene epoxide can be explained as the methyl rotation in **TS2** (Fig. 6). In *trans*-limonene epoxide, there is an equatorially oriented methyl group in the carbocation which after hydrogen transfer needs to rotate to keep both the stability and typical hybridization, leading exclusively to *trans*-DHC. Similarly, in *cis*-limonene epoxide, the methyl group in **TS2** rotates after the migration of hydrogen obtaining *cis*-DHC as the major product.

Additionally, an analysis of atoms in molecules was conducted for **TS2** to understand the nature of the hydrogen bond. For this purpose, the wavefunction was calculated, and various electronic variables (e.g., Laplacian of the electronic density ($\nabla^2 p(\mathbf{r})$) at the Bond Critical Point – BCP) were computed at the same level of theory. The positivity and negativity of the total energy density H(r) can indicate whether there is an ionic or covalent bond, circumventing issues with the Laplacian of the electronic density [45]. Furthermore, the combination of both $\nabla^2\rho(\mathbf{r})$ and H(**r**) can suggest the total or partial covalence of a bond. Depending on the signs of both, the interatomic distances in the compound can be categorized into three regions: Region I [$\nabla^2\rho(r) > 0$ and H(**r**) > 0 (purely closed-shell interactions)], region II [$\nabla^2\rho(\mathbf{r}) > 0$ and H(**r**) < 0 (closed-shell interactions with some covalent character)], and region III [$\nabla^2\rho(\mathbf{r}) < 0$ and H(**r**) < 0 (strong hydrogen bond and covalent bond) [46]. As observed in Fig. 5 for **TS2** (and Figure S2 and Table S2 in supporting information), both $\nabla^2\rho(\mathbf{r})$ and H(**r**) are negative. This indicates that such interactions can be associated with the presence of covalence in both bonds with no closed-shell interactions.

3.4. Kinetics

The mechanistic details obtained from the computational calculations helped to shed light on the reaction kinetics. The preliminary kinetic analysis using Eqs. (4) and (5) revealed that adsorption of all species had no significant influence on fitting the experimental data, except for *cis*-dihydrocarvone (C). Therefore, the final fitting involved the omission of constants K_A, K_B, K_D, K_E, and K_F in the denominator terms of Eqns. (4) and (5). Table S3 presents the optimized kinetic parameters for isomerization of limonene-1,2-epoxide. The reaction rate constants for reactions (4) and (6), estimated at 60 °C, exhibited the lowest values, consistent with the experimental results, where the primary reactions were identified as r_1 and r_2 involving formation of stereoisomers of dihydrocarvone. Conversely, reactions (7), (3), and (1) demonstrated the lowest activation energies, while reactions (4) and (6) displayed the highest energy barriers. This indicates that reactions (4) and (6) are not favorable under the tested conditions. In addition, the analysis indicates that formation of these dihydrocarvone isomers are the primary pathways which reinforce the notion that **int 2** formation is

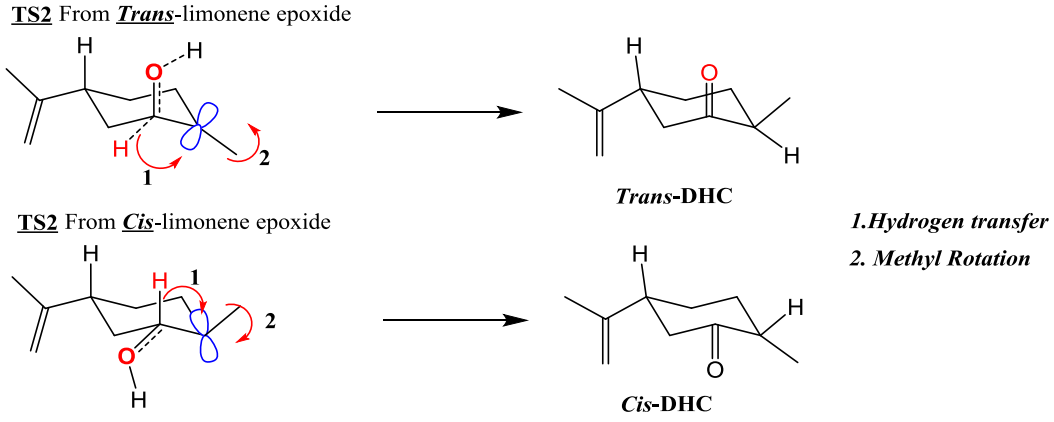

Fig. 6. Explanation for the diastereomeric selectivity in both *trans*- and *cis*-limonene epoxide.

crucial (showed during the computational calculations). The adsorption equilibrium constant for *cis*-dihydrocarvone over d-ZSM-5 was estimated to be 220 L/mol. The high adsorption equilibrium constant for *cis*-DHC suggests it binds more strongly to the catalyst, potentially affecting the final product distribution by influencing the conversion of the intermediate carbocation (Int2) to the specific DHC isomers. This aligns with the thermodynamic favorability discussed earlier. In summary, the kinetic analysis (reaction rates and activation energies from the previous section) suggests that the formation of both dihydrocarvone isomers (DHC and *trans*-carveol, TC) is limited more by kinetic factors than by thermodynamics which is also evident from the values of kinetic constants achieved through numerical data fitting and discussed below.

A large difference in the values of the activation energies E_{A1} and E_{A2} reflects the experimental observations of the cis/trans ratio dependence on temperature and can be also in part explained by the apparent compensation effect (a lower value of the pre-exponential factor k_2 compared to k_1 compensating for a higher activation energy).

On the other hand, Table S3 also indicates large errors for some of the parameters, which suggest that the associated catalytic reactions occur to a small extent (reactions (4), (6) and (7)). The comparison between experimental concentration profiles and those calculated with the kinetic model is illustrated in Figure S3. The results demonstrate that the proposed kinetics can effectively capture the behavior of the experimental data, yielding a high R^2 of 96.09 %. Furthermore, the statistical reliability of the constants was assessed through Markov Chain Monte Carlo (MCMC) analysis [40], as detailed in section 6 of the supporting information. The correlation between some parameters is depicted in contour plots. These plots reveal strong mutual correlations among certain parameters, as indicated by the presence of a few elongated ovals.

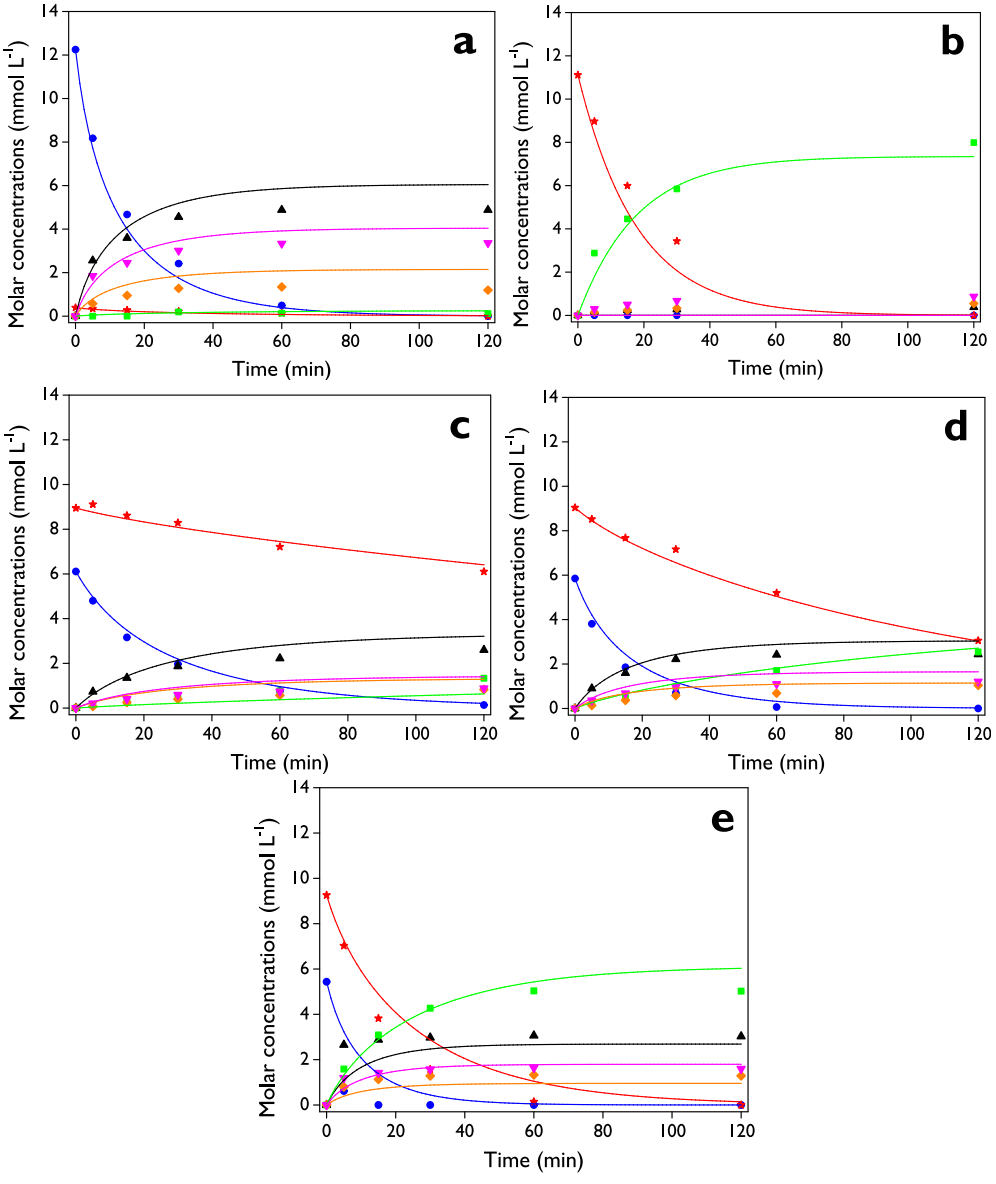

Fig. 7. Concentration profiles of the species (C_A (—, ●), C_B (—, ★), C_C (—, ▲), C_D (—, ■), C_E (—, ◆), C_F (—, ▼)) with the **refined model**, involved in the isomerization of limonene-1,2-epoxide over d-ZSM-5, with experimental values (symbols) and modeled values (solid lines). **Reaction conditions:** C_0 = 13 mmol/L, 75 mL total volume, anhydrous ethyl acetate as a solvent, 115 mg of catalyst, 520–530 rpm, N_2 atmosphere. **(a)** *cis*-LE as the substrate at 70 °C, **(b)** *trans*-LE as the substrate at 70 °C, **(c)** mixture-LE as the substrate at 50 °C, **(d)** mixture-LE as the substrate at 60 °C, **(e)** mixture-LE as the substrate at 70 °C.

Table 5
Optimized kinetic and statistical parameters for the refined kinetic model.

Parameter	Value	Units	Standard error (%)
k_1	$2.49x10^{-5}$	L mg^{-1} min^{-1}	9.3
k_2	$4.35x10^{-6}$	L mg^{-1} min^{-1}	6.1
k_3	$9.38x10^{-6}$	L mg^{-1} min^{-1}	7.0
k_5	$1.35x10^{-5}$	L mg^{-1} min^{-1}	7.7
k_8	$5.26x10^{-6}$	L mg^{-1} min^{-1}	7.3
Ea_1	41.1	kJ mol^{-1}	5.3
Ea_2	162.0	kJ mol^{-1}	11.2
Ea_3	35.5	kJ mol^{-1}	2.9
Ea_5	60.8	kJ mol^{-1}	5.8
Ea_8	80.2	kJ mol^{-1}	6.3
K_C	0.252	L $mmol^{-1}$	3.4

K_i values were estimated at 60 °C.

Based on the previous results of the robust kinetic model, large errors were obtained for the parameters related to reactions (4), (6), and (7) (Fig. 2). Therefore, the model was refined by suppressing these three reactions to achieve similar trends in the modeled kinetic curves shown in Figure S3, while reducing the number of parameters by six (3 k_i and 3 Ea_i). This adjustment aimed to lower the standard errors in the remaining kinetic parameters. The refined kinetic modeling was executed in ModEst considering $k_4 = k_6 = k_7 = 0$, resulting in almost the same quality of the fit ($R^2 = 94.72$ %) maintaining very similar trends in the kinetic curves, as illustrated in Fig. 7. Table 5 details the optimized parameters for the refined model, which now only requires 11 parameters compared to the previous 17 (as shown in Table S3). The highest standard error was observed for Ea_2, with a relatively low value of 11.2 %, indicating that the decision to suppress the three reactions was sound, leading to more accurate parameter values than previously obtained.

It is noteworthy to highlight that the kinetic parameters generally changed only slightly with the most significant change obtained for k_3. Additionally, note that the previously reported apparent activation energy (81 kJ mol^{-1}) was estimated using the initial rate of limonene epoxide consumption to all the products. Therefore, it cannot be directly compared with any of the values reported in Table 5, as each reaction has its own energy barrier.

Overall, in this work for dihydrocarvone synthesis a robust kinetic model was developed that includes all experimentally observed transformation routes over dendritic ZSM-5 zeolite as a heterogeneous catalyst. This is fundamental for future studies in scaling up batch processes for the synthesis of this fine chemical, as well as for optimizing different reaction conditions such as reaction temperature, initial substrate concentration, substrate source, and reaction time.

To our knowledge, this contribution is the first one reporting detailed kinetic modeling for limonene-1,2-epoxide isomerization based on the reaction rate laws for a dendritic zeolite as a heterogeneous catalyst. Although the literature on this topic is scarce, most studies highlight the absence of kinetic studies [1,18,20–22]. Cortés and Elrod [47] reported the kinetics of the hydrolysis of some monoterpene epoxides with D_2O, including pinene epoxides, (*cis-endo*, *trans-endo*)-limonene epoxide, and (*cis-endo*, *trans-endo*, *exo*)-limonene epoxide. The authors derived the rate equation according to a homogeneous kinetic model, which depends on the general acid-catalyzed rate constant (k_{GA}), the Brønsted acid-catalyzed rate constant (k_{H+}), and the concentration of the epoxide. However, in this contribution, the hydrolysis route was not considered because it was avoided by using anhydrous ethyl acetate and performing thermal treatment on the catalyst before the beginning of the reaction.

4. Conclusions

This study provides significant kinetic and mechanistic insights into the isomerization of limonene-1,2-epoxide over a dendritic ZSM-5 zeolite. This material demonstrated high selectivity and yield for forming dihydrocarvone (DHC) diastereoisomers due to its high accessibility, arising from its branched and radially oriented dendritic nanostructure and its balanced Brønsted/Lewis acidity. The use of ethyl acetate as a green solvent at a mild reaction temperature further underscores the environmentally friendly approach of this process. The study examined the effect of reaction temperature on LE conversion, showing that higher temperatures increased sharply the catalytic activity, with complete conversion achieved at 70 °C within 2 h, denoting the occurrence of a strongly activated process. Interestingly, the selectivity to DHC and carveol was not significantly affected by temperature.

Kinetic modeling for the isomerization of limonene-1,2-epoxide over d-ZSM-5 was proposed based on the reaction network with parallel reactions from *cis*-LE and *trans*-LE, assuming surface reactions as the rate-limiting steps. In this reaction pathway, *cis*-DHC was formed from *cis*-LE, while *trans*-DHC was obtained from *trans*-LE. The statistical results of this robust kinetic modeling highlighted the necessity to refine the model by suppressing three reactions. This adjustment led to a more accurate kinetic model with standard errors in all kinetic parameters reduced to below 11.2 %. The activation energies were determined to be 41.1 and 162 kJ/mol for *cis*-DHC and *trans*-DHC formation, respectively.

This kinetic modeling was supported by DFT calculations, which revealed the preferred pathway for both *cis* and *trans*-limonene epoxide conversion to dihydrocarvone and carveol. Thermodynamics favors formation of dihydrocarvone (both isomers) over the spontaneous generation of carveol. The rate-determining step, carbocation formation ($\Delta Eact = 234$ kJ mol^{-1}), precedes the nearly instantaneous formation of dihydrocarvone under the studied conditions. Analysis of the second transition state for DHC synthesis revealed closed-shell interactions with slight covalent character at the bond critical point. This finding is consistent with the experimental results, supporting the overall DFT profile.

CRediT authorship contribution statement

Luis A. Gallego-Villada: Writing – original draft, Methodology, Investigation, Conceptualization. **Wander Y. Perez-Sena:** Investigation, Formal analysis. **Julián E. Sánchez-Velandia:** Writing – original draft, Software, Investigation. **Jennifer Cueto:** Investigation. **María del Mar Alonso-Doncel:** Writing – review & editing, Investigation. **Johan Wärmå:** Investigation. **Päivi Mäki-Arvela:** Writing – review & editing, Supervision. **Edwin A. Alarcón:** Writing – review & editing, Supervision, Funding acquisition. **David P. Serrano:** Writing – review & editing, Supervision, Conceptualization. **Dmitry Yu Murzin:** Writing – review & editing, Supervision, Project administration, Methodology.

Declaration of competing interest

The authors declare that they have no known competing financial interests or personal relationships that could have appeared to influence the work reported in this paper.

Data availability

Data will be made available on request.

Acknowledgments

Luis A. Gallego-Villada is grateful to Universidad de Antioquia for their support during his research internship through the project 2022-53000 as part of the “Convocatoria Programática 2021-2022: Ingeniería y Tecnología” program, as well as the “Beca Doctoral Universidad de Antioquia” scholarship. D.P.S., M.A-D., and J.C. are gratefully acknowledged to the European Research Council Horizon 2020 research and innovation program TODENZE project (ERC101021502). Julián E. Sánchez-Velandia is grateful to Universidad Jaume I for the postdoctoral position during 2022-2023 (programa Propi UJI) and the project

(PID2020-11962RBC33),MCIN/AEI/10.13039/501100011033/European Union NextGeneration EU/PRTP.

Appendix A. Supplementary data

Supplementary data to this article can be found online at https://doi.org/10.1016/j.cej.2024.155377.

References

[1] R.F. Cotta, R.A. Martins, M.M. Pereira, K.A. da Silva Rocha, E.F. Kozhevnikova, I. V. Kozhevnikov, E.V. Gusevskaya, Heteropoly acid catalysis for the isomerization of biomass-derived limonene oxide and kinetic separation of the trans-isomer in green solvents, Appl. Catal. A Gen. 584 (2019) 117173, https://doi.org/10.1016/j.apcata.2019.117173.

[2] Foreverest, Dihydrocarvone, (n.d.). https://foreverest.net/products/turpentine-derivatives/dihydrocarvone.html (accessed November 12, 2023).

[3] A.R. Alcántara, M.-J. Hernaiz, J.-V. Sinisterra, Biocatalyzed production of fine chemicals, in, Compr. Biotechnol., Second Edi, Elsevier (2011) 309–331, https://doi.org/10.1016/B978-0-08-088504-9.00225-7.

[4] J.E. Sánchez-Velandia, L.A. Gallego-Villada, P. Mäki-Arvela, A. Sidorenko, D. Yu, Murzin, Upgrading biomass to high-added value chemicals: synthesis of monoterpenes-based compounds using catalytic green chemical pathways, Catal. Rev. (2024) 1–126, https://doi.org/10.1080/01614940.2024.2329553.

[5] V.M. Vaschetti, A.L. Cánepa, D. Barrera, K. Sapag, G.A. Eimer, S.G. Casuscelli, Limonene oxyfunctionalization over Cu-modified silicates employing hydrogen peroxide and t-butyl hydroperoxide: Reaction pathway analysis, Mol. Catal. 481 (2020) 110234, https://doi.org/10.1016/j.mcat.2018.11.005.

[6] M. Caovilla, A. Caovilla, S.B.C. Pergher, M.C. Esmelindro, C. Fernandes, C. Dariva, K. Bernardo-Gusmão, E.G. Oestreicher, O.A.C. Antunes, Catalytic oxidation of limonene, α-pinene and β-pinene by the complex [FeIII(BPMP)Cl(μ-O)FeIIICl3] biomimetic to MMO enzyme, Catal. Today. 133–135 (2008) 695–698, https://doi.org/10.1016/j.cattod.2007.12.107.

[7] L.A. Gallego-Villada, E.A. Alarcón, A.L. Villa, Versatile heterogeneous catalytic system for the selective synthesis of limonene epoxide and diepoxide, Ind. Eng. Chem. Res. 62 (2023) 20152–20169, https://doi.org/10.1021/acs.iecr.3c02633.

[8] L.A. Gallego-Villada, P. Mäki-Arvela, N. Kumar, E.A. Alarcón, Z. Vajglová, T. Tirri, I. Angervo, R. Lassfolk, M. Lastusaari, D.Y. Murzin, Zeolite Y-based catalysts for efficient epoxidation of R-(+)-limonene: Insights into the structure-activity relationship, Microporous Mesoporous Mater. 372 (2024) 113098, https://doi.org/10.1016/j.micromeso.2024.113098.

[9] M. Vasconcellos-Dias, C.D. Nunes, V. Félix, P. Brandão, M.J. Calhorda, New heptacoordinate tungsten(II) complexes with α-diimine ligands in the catalytic oxidation of multifunctional olefins, Inorganica Chim. Acta. 519 (2021) 120263, https://doi.org/10.1016/j.ica.2021.120263.

[10] H. Zhang, X. Lu, L. Yang, Y. Hu, M. Yuan, C. Wang, Q. Liu, F. Yue, D. Zhou, Q. Xia, Efficient air epoxidation of cycloalkenes over bimetal-organic framework ZnCo-MOF materials, Mol. Catal. 499 (2021) 111300, https://doi.org/10.1016/j.mcat.2020.111300.

[11] Y.S. Demidova, E.V. Suslov, O.A. Simakova, K.P. Volcho, N.F. Salakhutdinov, I. L. Simakova, D.Y. Murzin, Selective one-pot carvone oxime hydrogenation over titania supported gold catalyst as a novel approach for dihydrocarvone synthesis, J. Mol. Catal. A Chem. 420 (2016) 142–148, https://doi.org/10.1016/j.molcata.2016.04.013.

[12] J.R. Lowe, W.B. Tolman, M.A. Hillmyer, Oxidized dihydrocarvone as a renewable multifunctional monomer for the synthesis of shape memory polyesters, Biomacromolecules 10 (2009) 2003–2008, https://doi.org/10.1021/bm900471a.

[13] J.M. Kouznetsov, V. Vladímir, G. Urbina, E.E. Stashenko, N-Functionalization of dihydrocarvone: Obtainin aminocyclohexane derivatives and their spectrometric study, J. Chil. Chem. Soc. 50 (2005) 559–563.

[14] Y. Dong, K.J. McCullough, S. Wittlin, J. Chollet, J.L. Vennerstrom, The structure and antimalarial activity of dispiro-1,2,4,5-tetraoxanes derived from (+)-dihydrocarvone, Bioorg. Med. Chem. Lett. 20 (2010) 6359–6361, https://doi.org/10.1016/j.bmcl.2010.09.113.

[15] J. Alarcon, C. Lamilla, C.L. Cespedes, Insecticidal activity of sesquiterpenes skeleton synthesized by the conventional Robinson annulations reaction on Drosophila melanogaster, Ind. Crops Prod. 42 (2013) 268–272, https://doi.org/10.1016/j.indcrop.2012.05.026.

[16] M. Stekrova, N. Kumar, S.F. Díaz, P. Mäki-Arvela, D.Y. Murzin, H- and Fe-modified zeolite beta catalysts for preparation of trans-carveol from α-pinene oxide, Catal. Today. 241 (2015) 237–245, https://doi.org/10.1016/j.cattod.2013.12.004.

[17] S.P. Bhatia, D. McGinty, C.S. Letizia, A.M. Api, Fragrance material review on carveol, Food Chem. Toxicol. 46 (2008) S85–S87, https://doi.org/10.1016/j.fct.2008.06.032.

[18] T.-T.-T. Nguyen, D.-K.-N. Chau, F. Duus, T.N. Le, Green synthesis of carvenone by montmorillonite-catalyzed isomerization of 1,2-limonene oxide, Int. J. Org. Chem. 03 (2013) 206–209, https://doi.org/10.4236/ijoc.2013.33027.

[19] A. Corma, S. Iborra, A. Velty, Chemical routes for the transformation of biomass into chemicals, Chem. Rev. 107 (2007) 2411–2502, https://doi.org/10.1021/cr050989d.

[20] N. Ravasio, F. Zaccheria, M. Guidotti, R. Psaro, Mono- and bifunctional heterogeneous catalytic transformation of terpenes and terpenoids, Top. Catal. 27 (2004) 157–168, https://doi.org/10.1023/B:TOCA.0000013550.28170.6a.

[21] V.V. Costa, K.A. da Silva Rocha, I.V. Kozhevnikov, E.F. Kozhevnikova, E. V. Gusevskaya, Heteropoly acid catalysts for the synthesis of fragrance compounds from biorenewables: isomerization of limonene oxide, Catal. Sci. Technol. 3 (2013) 244–250, https://doi.org/10.1039/C2CY20526B.

[22] J.E. Sánchez-Velandia, A.L. Villa, Selective synthesis of high-added value chemicals from α-pinene epoxide and limonene epoxide isomerization over mesostructured catalysts: Effect of the metal loading and solvent, Catal. Today. 394–396 (2022) 208–218, https://doi.org/10.1016/j.cattod.2021.09.011.

[23] C. Raptis, H. Garcia, M. Stratakis, Selective isomerization of epoxides to allylic alcohols catalyzed by TiO_2 -supported gold nanoparticles, Angew. Chemie Int. Ed. 48 (2009) 3133–3136, https://doi.org/10.1002/anie.200805838.

[24] K. Arata, S. Akutagawa, K. Tanabe, Isomerization of d-limonene oxide over solid acids and bases, J. Catal. 41 (1976) 173–179, https://doi.org/10.1016/0021-9517(76)90213-X.

[25] L.A. Gallego-Villada, J. Cueto, M.del M. Alonso-Doncel, P. Mäki-Arvela, E. A. Alarcón, D.P. Serrano, D.Y. Murzin, Dendritic ZSM-5 zeolites as highly active catalysts for the valorization of monoterpene epoxides (submitted), Green Chem. (2024).

[26] M. del Mar Alonso-Doncel, C. Ochoa-Hernández, G. Gómez-Pozuelo, A. Oliveira, J. González-Aguilar, Á. Peral, R. Sanz, D.P. Serrano, Dendritic nanoarchitecture imparts ZSM-5 zeolite with enhanced adsorption and catalytic performance in energy applications, J. Energy Chem. 80 (2023) 77–88, https://doi.org/10.1016/j.jechem.2023.01.023.

[27] M. del M. Alonso-Doncel, E.A. Giner, D. de la Calle, J. Cueto, P. Horcajada, R. A. García-Muñoz, D.P. Serrano, Synthesis of dendritic ZSM-5 Zeolite through micellar templating controlled by the amphiphilic organosilane chain length, Cryst. Growth Des. 23 (2023) 5658–5670, https://doi.org/10.1021/acs.cgd.3c00326.

[28] M. Alonso-Doncel, A. Peral, M. Shamzhy, J. Čejka, R. Sanz, D.P. Serrano, Untangling the role of the organosilane functional groups in the synthesis of hierarchical ZSM-5 zeolite by crystallization of silanized protozeolitic units, Catal. Today. 345 (2020) 27–38, https://doi.org/10.1016/j.cattod.2019.11.031.

[29] N. Kumar, P. Mäki-Arvela, S.F. Diáz, A. Aho, Y. Demidova, J. Linden, A. Shepidchenko, M. Tenhu, J. Salonen, P. Laukkanen, A. Lashkul, J. Dahl, I. Sinev, A. Leino, K. Kordas, T. Salmi, D.Y. Murzin, Isomerization of α-pinene oxide over iron-modified zeolites, Top. Catal. 56 (2013) 696–713, https://doi.org/10.1007/s11244-013-0029-y.

[30] D.Y. Murzin, T. Salmi, Catalytic kinetics, 1st ed.,, ElSevier Science & Technology Books, 2005.

[31] L. Lu, H. Hu, H. Hou, B. Wang, An improved B3LYP method in the calculation of organic thermochemistry and reactivity, Comput. Theor. Chem. 1015 (2013) 64–71, https://doi.org/10.1016/j.comptc.2013.04.009.

[32] S. Grimme, J. Antony, S. Ehrlich, H. Krieg, A consistent and accurate ab initio parametrization of density functional dispersion correction (DFT-D) for the 94 elements H-Pu, J. Chem. Phys. 132 (2010), https://doi.org/10.1063/1.3382344.

[33] W. Reckien, F. Janetzko, M.F. Peintinger, T. Bredow, Implementation of empirical dispersion corrections to density functional theory for periodic systems, J. Comput. Chem. 33 (2012) 2023–2031, https://doi.org/10.1002/jcc.23037.

[34] B. Civalleri, C.M. Zicovich-Wilson, L. Valenzano, P. Ugliengo, B3LYP augmented with an empirical dispersion term (B3LYP-D*) as applied to molecular crystals, CrstEngComm 10 (2008) 405–410, https://doi.org/10.1039/B715018K.

[35] Y. Shao, Y. Mei, D. Sundholm, V.R.I. Kaila, Benchmarking the performance of time-dependent density functional theory methods on biochromophores, J. Chem. Theory Comput. 16 (2020) 587–600, https://doi.org/10.1021/acs.jctc.9b00823.

[36] Y. Takano, K.N. Houk, Benchmarking the conductor-like polarizable continuum model (CPCM) for aqueous solvation free energies of neutral and ionic organic molecules, J. Chem. Theory Comput. 1 (2005) 70–77, https://doi.org/10.1021/ct049977a.

[37] B. Lasne, P. Mäki-Arvela, A. Aho, Z. Vajglova, K. Eränen, N. Kumar, J.E. Sánchez-Velandia, M. Peurla, C. Mondelli, J. Pérez-Ramírez, D.Y. Murzin, Synthesis of florol via prins cyclization over heterogeneous catalysts, J. Catal. 405 (2022) 288–302, https://doi.org/10.1016/j.jcat.2021.12.008.

[38] L.A. Gallego-Villada, E.A. Alarcón, D.M. Ruiz, G.P. Romanelli, Kinetic study of the esterification of t-cinnamic acid over preyssler structure acid, Mol. Catal. 528 (2022) 112507, https://doi.org/10.1016/j.mcat.2022.112507.

[39] L.A. Gallego-Villada, E.A. Alarcón, C. Cerrutti, G. Blustein, Á.G. Sathicq, G. P. Romanelli, Levulinic acid esterification with n -butanol over a Preyssler catalyst in a microwave-assisted batch reactor: A kinetic study, Ind. Eng. Chem. Res. 62 (2023) 10915–10929, https://doi.org/10.1021/acs.iecr.3c00893.

[40] D.Y. Murzin, J. Wärnå, H. Haario, T. Salmi, Parameter estimation in kinetic models of complex heterogeneous catalytic reactions using Bayesian statistics, React. Kinet. Mech. Catal. 133 (2021) 1–15, https://doi.org/10.1007/s11144-021-01974-1.

[41] H. Haario, ModEst user's guide, ProfMath Oy, Helsinki, 1994.

[42] W.H. Thompson, Quantum mechanical transition state theory and tunneling corrections, J. Chem. Phys. 110 (1999) 4221–4228, https://doi.org/10.1063/1.478304.

[43] R.G. Pearson, Hard and soft acids and bases, J. Am. Chem. Soc. 85 (1963) 3533–3539, https://doi.org/10.1021/ja00905a001.

[44] R.G. Pearson, Recent advances in the concept of hard and soft acids and bases, J. Chem. Educ. 64 (1987) 561, https://doi.org/10.1021/ed064p561.

[45] D.K. Miller, C. Loy, S.V. Rosokha, Examining a transition from supramolecular halogen bonding to covalent bonds: Topological analysis of electron densities and

energies in the complexes of bromosubstituted electrophiles, ACS Omega 6 (2021) 23588–23597, https://doi.org/10.1021/acsomega.1c03779.
[46] R. Bianchi, G. Gervasio, D. Marabello, The experimental charge density in transition metal compounds, Comptes Rendus Chim. 8 (2005) 1392–1399, https://doi.org/10.1016/j.crci.2004.12.015.
[47] A. Di, M.J.E. Cortés, Kinetics of the aqueous phase reactions of atmospherically relevant monoterpene epoxides, J. Phys. Chem. a. 121 (2017) 9297–9305, https://doi.org/10.1021/acs.jpca.7b09427.